Mineralogical Magazine, December 2014, Vol. 78(7), pp. 1763–1773

Crystal structure and revised chemical formula for burckhardtite, $Pb_2(Fe^{3+}Te^{6+})[AlSi_3O_8]O_6$: a double-sheet silicate with intercalated phyllotellurate layers

ANDREW G. CHRISTY[1,*], ANTHONY R. KAMPF[2], STUART J. MILLS[3], ROBERT M. HOUSLEY[4] AND BRENT THORNE[5]

[1] Centre for Advanced Microscopy, Australian National University, Canberra, ACT 0200, Australia
[2] Mineral Sciences Department, Natural History Museum of Los Angeles County, 900 Exposition Boulevard, Los Angeles, CA 90007, USA
[3] Geosciences, Museum Victoria, GPO Box 666, Melbourne 3001, Victoria, Australia
[4] Division of Geological and Planetary Sciences, California Institute of Technology, Pasadena, CA 91125, USA
[5] 3898 S. Newport Circle, Bountiful, UT 84010, USA

[*Received 5 May 2014; Accepted 27 June 2014; Associate Editor: E. Grew*]

ABSTRACT

The crystal structure of burckhardtite from the type locality, Moctezuma, Sonora, Mexico, has been refined to $R_1 = 0.0362$ and w$R_2 = 0.0370$ for 215 reflections with $I > 2\sigma(I)$. Burckhardtite is trigonal, space group $P\bar{3}1m$, with the unit-cell parameters $a = 5.2566(5)$ Å, $c = 13.0221(10)$ Å, $V = 311.62(5)$ Å^3 and $Z = 1$ for the ideal formula unit $Pb_2(Fe^{3+}Te^{6+})[AlSi_3O_8]O_6$. There is no long-range order of (Fe^{3+}, Te^{6+}) or (Al^{3+}, Si^{4+}). New microprobe data were used to estimate site scattering factors, and Raman spectroscopic data showed no evidence of O–H stretching bands. Burckhardtite is not closely related to the micas, as supposed previously, but is a double-sheet silicate in which the aluminosilicate anion resembles that of minerals such as cymrite and kampfite. The $[(Fe^{3+}Te^{6+})O_6]^{3-}$ part of the structure is not bonded directly to the aluminosilicate layer, but forms a discrete anionic phyllotellurate layer that alternates with the $[AlSi_3O_8]^-$ double sheets. Similar phyllotellurate layers are known from several synthetic phases. In burckhardtite, Pb^{2+} cations intercalate between phyllosilicate and phyllotellurate layers, forming a $Pb_2[FeTeO_6]$ module that is topologically similar to a slab of the structure of rosiaite, $Pb[Sb_2O_6]$. The crystal symmetry, structure, classification as a double-sheet silicate and chemical formula, including the determination of the 6+ valence of Te and absence of essential H_2O, are all new findings for the mineral.

KEYWORDS: crystal structure, burckhardtite, phyllotellurate, phyllosilicate, double-sheet silicate, Moctezuma.

Introduction

BURCKHARDTITE, was originally described from the Moctezuma mine (Bambolla mine) in Sonora, Mexico by Gaines *et al.* (1979) as a silicate–tellurite with the formula $Pb_2(Fe^{3+},Mn^{3+})Te^{4+}(AlSi_3O_{10})O_2(OH)_2{\cdot}H_2O$. Crystals occur as carmine-red platelets up to 20 μm across and are intergrown to form larger rosettes up to 0.1 mm across. Burckhardtite is an extremely rare mineral and has been observed only in two other localities: the Bird Nest drift on Otto Mountain, Baker, California (Kampf *et al.*, 2010) and the Reef mine, Carr Canyon, Arizona (Walstrom, 2012). Because of the small amount of single-phase material available, Gaines *et al.* (1979) had to make several assumptions about the mineral: (1) the valence of Te was assumed to be 4+ based on the association with paratellurite, moctezumite and zemannite; (2) H_2O was taken to be a significant constituent, as estimated by difference of the EMPA microprobe analyses from 100 wt.% total; (3) burckhardtite was assumed to be

* E-mail: Andrew.Christy@anu.edu.au
DOI: 10.1180/minmag.2014.078.7.18

C-centred monoclinic by analogy with micas. Gaines *et al*. (1979) estimated unit-cell parameters as $a = 5.21$ Å, $b = 9.04$ Å, $c = 12.85$ Å and $\beta = 90^{\circ}$, but noted that "a number of minor lines fail to index readily", supporting the need for further study. On the basis of the assumed relationship to micas, a structure was proposed, based on sheets of $[Pb_2FeTeO_2{\cdot}H_2O]^{7+}$ or $[Pb_2FeTeO(OH)_2]^{7+}$, sandwiched between a pair of mica-like sheets of composition $[AlSi_3O_{10}(OH)_2]^{7-}$. Given the unverified assumptions in the characterization of the mineral to date, its interest as a possible Te-bearing mica analogue, and as part of our greater study on the crystallography and chemistry of Te oxysalts (Mills and Christy, 2013; Christy and Mills, 2013), we have re-examined crystals of burckhardtite from the Moctezuma mine and report the results of the structure investigation, along with new analytical data which we have compared with those of Gaines *et al.* (1979). The crystals used in this study were obtained from two small fragments removed from a larger specimen, a portion of which is shown in Fig. 1. These are preserved in the collections of the Natural History Museum of Los Angeles County, catalogue number 64173.

Experimental

Electron microprobe analysis

Electron microprobe (EMP) analyses for the burckhardtite sample used in this study were obtained on a JEOL8200 microprobe at the California Institute of Technology, using 15 kV accelerating voltage, 2 μm spot size and 5 nA probe current. Standards used were: anorthite (Al, Si and Ca), forsterite (Mg), synthetic Mn olivine (Mn), fayalite (Fe), galena (S and Pb), benitoite (Ba) and pure elements for Cu, Se and Te. The elements Mg, Cu, Se and Ba were always below detection limits. The Raman spectrum (see section below) showed no evidence of unanalysed light components such as CO_3 or H_2O. The variable-valence elements Mn, Fe and Te are expressed as Mn_2O_3, Fe_2O_3 and TeO_3, consistent with the strong purple-red colour attributable to Mn^{3+} (Fig. 1) and the bond-valence sums of the structure refinement (see section below). Analyses were recalculated to 14 oxygen atoms, consistent with the structure refinement. Data are summarized in Table 1, and are broadly in agreement with those of Gaines *et al*. (1979). The mounted grains were polycrystalline and porous, which accounts for the low totals. The structure refinement indicates an ideal stoichiometry $A_2M_2[T_4O_8]O_6$, where A = asymmetrically-coordinated large cation (mainly Pb^{2+}), M = octahedrally-coordinated cation (mainly Te^{6+} and Fe^{3+}) and T = tetrahedrally-coordinated cation (mainly Si and Al). If (Al+Si+S) are placed on T, (Te+Fe+Mn) on M and (Pb+Ca) on A sites, the mean of the 7 EMP analyses of this present study gives the formula $(Pb_{1.76}Ca_{0.05})_{\Sigma 1.81}(Te^{6+}_{1.13}Fe^{3+}_{0.83}Mn^{3+}_{0.24})_{\Sigma 2.20}[(Si_{2.85}Al_{0.97}S_{0.01})_{\Sigma 3.83}O_8]O_6$. The analyses show considerable variation in the ratio of (Te+Fe+Mn):(Si+Al) and a consistent deficiency of Pb; such problems are common with EMPA of heavy elements, and may be due to extreme ZAF correction factors needed with the standards available. However, we note that Al:(Al+Si) and Te:(Fe+Mn) ratios were always close to 1:3 and 1:1 respectively, consistent with the ideal formula $Pb_2(Fe^{3+}Te^{6+})[AlSi_3O_8]O_6$ derived from the structure refinement.

Raman spectroscopy

Raman spectra were obtained with a Renishaw M-1000 microRaman spectrometer system with a 514.3 nm Cobalt solid-state laser operating at 10% power through a 100× objective that produced 0.6 mW on an ~1 μm diameter spot on the mounted and polished sample used for microprobe analysis.

The spectrum of burckhardtite is dominated by a strong band at 690 cm^{-1}, attributed to the ν_1 symmetric stretching mode of TeO_6. This band occurs in the centre of the 615–810 cm^{-1} range

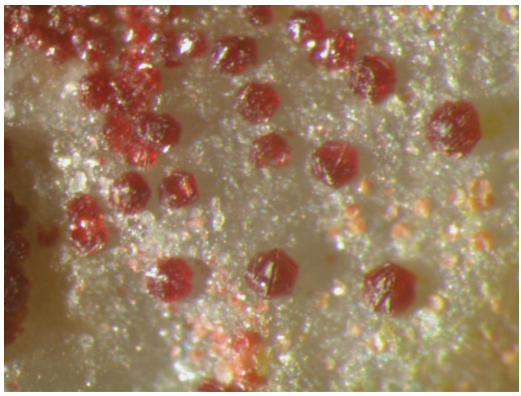

FIG. 1. Rosettes of hexagonal burckhardtite tablets with pearly-white flakes of probable dickite, on the specimen used in this study. Field of view = 1 mm.

TABLE 1. Electron microprobe analyses of burckhardtite.

Oxide	– This study (seven spots) – Mean wt.%	Range wt.%	Gaines *et al.* (1979) Wt.%
TeO_3	20.86	18.18–20.86	18.74*
SO_3	0.12	0–0.32	–
SiO_2	17.91	16.86–19.35	20.28
Al_2O_3	5.19	4.79–5.70	5.44
Fe_2O_3	6.91	6.27–7.47	7.25
Mn_2O_3	1.98	1.42–2.51	1.18
CaO	0.29	0.12–0.53	–
PbO	41.18	38.62–43.08	45.23
Total	94.43	93.35–95.15	96.41†
Recalculated to 14 oxygens			
Si	2.85	2.68–3.08	3.12
Al	0.97	0.90–1.07	0.98
S	0.01	0–0.04	–
Fe	0.83	0.75–0.90	0.84
Mn	0.24	0.17–0.31	0.14
Te	1.13	0.99–1.25	0.99
Pb	1.76	1.65–1.85	1.87
Ca	0.05	0.02–0.09	–
Al/(Al+Si)	0.254	0.251–0.258	0.239
Te/(Te+Fe+Mn)	0.516	0.505–0.527	0.503
Mn/(Fe+Mn)	0.225	0.172–0.270	0.143

* Recalculated from TeO_2 equivalent.
† Not including assumed H_2O.

expected for such vibrations, and is very close to the strong 694 cm^{-1} observed for mojaveite, $Cu_6[Te^{6+}O_4(OH)_2](OH)_7Cl$ (Mills *et al.*, 2014), which also contains $Te(O,OH)_6$ octahedra as components in an edge-sharing octahedral sheet. Additional strong bands in the burckhardtite spectrum at 646 and 619 cm^{-1} and a weak feature at 661 cm^{-1} may be compared with mojaveite bands at 654 and 624 cm^{-1}. The spectrum of bairdite, $Pb_2Cu_4^{2+}Te_2^{6+}O_{10}(OH)_2(SO_4)(H_2O)$, is similarly dominated by a tellurate mode at 721 cm^{-1} (Kampf *et al.*, 2013*a*) and that of eckhardite, $(Ca,Pb)Cu^{2+}Te^{6+}O_5(H_2O)$, by peaks at 729 and 692 cm^{-1} (Kampf *et al.*, 2013*b*).

Lower-frequency peaks in the Raman spectrum of burckhardtite were observed at 554, 477 (with shoulders at ~463 and 505), 391, 322, 295 and 202 cm^{-1}. These will include tellurate and aluminosilicate bending modes. Stretching modes of the aluminosilicate anion gave only weak bands at 833 and 897 cm^{-1}. The bands may be compared with those in the corresponding wavenumber region for other double-sheet phyllosilicates. Cymrite, $Ba[Al_2Si_2O_8]\cdot H_2O$, has weak peaks at 800 and 953 cm^{-1} (Graham *et al.*, 1992), while aluminosilicate stretches for 'K-cymrite', $K[AlSi_3O_8]\cdot H_2O$ and kokchetavite, $K[AlSi_3O_8]$, are at 832.5 and 800 cm^{-1}, respectively (Kanzaki *et al.*, 2012) and for dmisteinbergite, $Ca[Al_2Si_2O_8]$, at 912, 893 and 801 cm^{-1} (Fintor *et al.*, 2013).

No bands attributable to O–H were seen in the 2500–4000 cm^{-1} region, consistent with the absence of significant OH^- or H_2O deduced from the structure refinement (see below).

Powder diffraction

X-ray diffraction data for burckhardtite were obtained on a Rigaku R-Axis Rapid II curved imaging plate microdiffractometer utilizing monochromatized MoK_α radiation. The observed powder *d*-spacings and intensities were derived by profile fitting using *JADE 2010* software (Materials Data, Inc.). Unit-cell parameters

refined from the powder data using *JADE 2010* with whole pattern fitting are: a = 5.2540(4) Å and c = 13.0121(12) Å. The observed d spacings fit well with those calculated from the structure and those reported by Gaines *et al*. (1979) (Table 2).

Single-crystal X-ray diffraction

Single-crystal data were collected on the same instrument noted above at 293 K, using a crystal fragment ~35 μm × 25 μm × 10 μm in size. The Rigaku *CrystalClear* software package was used

TABLE 2. Powder X-ray data for burckhardtite (d spacings in Å).

This study		Based on structure – This study			Gaines *et al*. (1979)	
I_{obs}	d_{obs}	I_{calc}	d_{calc}	$h\ k\ l$	I_{obs}	d_{obs}
83	13.03	99	13.0221	0 0 1	90	12.80
		1	6.5111	0 0 2		
17	4.547	13	4.5523	1 0 0	20	4.51
18	4.294	14	4.2973	1 0 1	20	4.26
81	3.730	76	3.7309	1 0 2	90	3.70
100	3.141	100	3.1415	1 0 3	100	3.11
		1	2.6481	1 0 4		
60	2.627	48	2.6283	1 1 0	70	2.60
		7	2.6044	0 0 5		
10	2.578	9	2.5763	$\bar{1}\ \bar{1}\ 1$	10	2.56
4	2.433	3	2.4372	1 1 2	10	2.42
29	2.262	9	2.2762	2 0 0	30	2.26
		10	2.2606	1 0 5		
		6	2.2483	1 1 3	30	2.24
		2	2.2422	2 0 1		
30	2.151	6	2.1704	0 0 6	10	2.16
		21	2.1487	2 0 2	30	2.13
		1	2.0450	$\bar{1}\ \bar{1}\ 4$	5	2.04
21	2.0164	18	2.0158	2 0 3	20	2.00
5	1.9557	4	1.9591	1 0 6	5	1.952
		2	1.8654	2 0 4		
38	1.8497	33	1.8500	$\bar{1}\ \bar{1}\ 5$	60	1.840
		1	1.7221	1 0 7		
8	1.7148	3	1.7206	2 1 0		
		2	1.7139	2 0 5		
		2	1.7058	$\bar{2}\ \bar{1}\ 1$		
33	1.6680	17	1.6735	$\bar{1}\ \bar{1}\ 6$		
		16	1.6635	$\bar{2}\ \bar{1}\ 2$		
29	1.5992	27	1.5995	$\bar{2}\ \bar{1}\ 3$	50	1.590
3	1.5684	3	1.5707	2 0 6	5	1.563
12	1.5309	12	1.5327	1 0 8	20	1.526
		1	1.5212	2 1 4		
17	1.5155	13	1.5175	3 0 0	20	1.508
		4	1.5073	3 0 1		
5	1.4356	1	1.4404	2 0 7		
		4	1.4356	2 1 5	5	1.426
		1	1.4324	3 0 3		
		2	1.3789	1 0 9	5	1.371
		2	1.3483	2 1 6	5	1.340
8	1.3233	9	1.3240	2 0 8	10	1.318
15	1.3120	7	1.3142	2 2 0	20	1.306
		7	1.3111	3 0 5		

Only lines with d >1.3 Å are included.

TABLE 3. Assigned site-distribution scheme for burckhardtite, $AM_2[T_4O_8]O_6$, comparing electron counts estimated from atomic proportions in mean microprobe analysis and those from X-ray diffraction structure refinement.

Site	Population	e^-_{EMPA}	e^-_{XRD}
A	$(Pb_{0.97}Ca_{0.03})$	80.1	80.5(25)
M	$(Te_{0.51}Fe_{0.38}Mn_{0.11})$	39.2	37.9(10)
T	$(Si_{0.75}Al_{0.25})$	13.75	13.8(6)

for processing of the diffraction data, including the application of an empirical multi-scan absorption correction using *ABSCOR* (Higashi, 2001). The structure was solved in space group $P\bar{3}1m$ (No. 162) by direct methods using *SIR2004* (Burla *et al*., 2005). *SHELXL-2013* (Sheldrick, 2008) was used for the refinement of the structure. Initially, occupancies were refined for Pb on *A*, Te on *M* and Si on *T*, so as to estimate overall site scattering factors for the mixed species on these sites. The electron counts were found to agree closely with those calculated if site populations were as in the formula recalculated from the averaged microprobe data above. Species were assigned in these proportions so as to fully occupy sites for the final refinement (Table 3), analogous to the method of Mills *et al*. (2012*a*). Neutral-atom scattering curves were used (Ibers and Hamilton, 1974). The final model, with all atomic displacement parameters refined anisotropically, converged to $R_1 = 0.0362$ for 215 observed reflections [$I_o > 2\sigma I$] and 0.0370 for all 223 unique reflections. Data collection and structure refinement details are provided in Table 4. The largest difference peak, 3.375 e/Å^3, is only 1.13 Å from Pb. Other positive difference peaks are too small to suggest the presence of significant additional components such as H_2O. Atomic coordinates and displacement parameters are in Table 5, selected bond distances in Table 6 and bond-valence sums in Table 7. For bond-valence calculations, the cation-site occupancies of Table 3 were used, and bond values were calculated using appropriately weighted averages of those for the respective substituents. Bond-valence parameters used were those of Brese and O'Keeffe (1991) except for Pb^{2+}–O (r_0 = 1.963 Å, b = 0.49 Å: Krivovichev and Brown, 2001) and Te^{6+}–O (r_0 = 1.921 Å, b = 0.56 Å: Mills and Christy, 2013). All bond-valence sums for oxygen atoms are very close to 2 (1.89–2.05 valence units) and would only

TABLE 4. Crystal data and structure refinement for burckhardtite.

Ideal formula	$Pb_2(Fe^{3+}Te^{6+})[AlSi_3O_8]O_6$
Temperature	293(2) K
Wavelength	0.71075 Å
Space group	$P\bar{3}1m$
Unit-cell dimensions	a = 5.2566(5) Å
	c = 13.0221(10) Å
Volume	311.62(5) Å^3
Z	1
Crystal size (μm)	35 × 25 × 10
Absorption coefficient (mm^{-1})	30.033
F(000)	405
Theta range for data collection	3.13 to 24.90°
Index ranges	$-5 \leqslant h \leqslant 5$, $-6 \leqslant k \leqslant 6$, $-15 \leqslant l \leqslant 15$
Independent reflections	1667 [R_{int} = 0.0316]
Refinement method	Full-matrix least-squares on F^2
Data / restraints / parameters	223 / 0 / 25
Reflections with $I > 2\sigma(I)$	215
Gof on F^2	1.249
Final R indices [$I > 2\sigma(I)$]	R_1 = 0.0362, wR_2 = 0.0772
R indices (all data)	R_1 = 0.0370, wR_2 = 0.0775
Extinction coefficient	None
Largest diff. peak and hole (e/Å^3)	3.375 and −2.134

TABLE 5. Atom coordinates and displacement parameters (Å^2) for burckhardtite.

Site	Occupancy	*x*/*a*	*y*/*b*	*z*/*c*	U_{eq}	U^{11}	U^{22}	U^{33}	U^{23}	U^{13}	U^{12}
A	0.97Pb + 0.03Ca	1	0	0.31612(9)	0.0146(4)	0.0141(5)	0.0141(5)	0.0155(6)	0	0	0.0072(2)
M	0.51Te + 0.38Fe + 0.11Mn	⅔	⅓	½	0.0124(6)	0.0086(8)	0.0086(8)	0.0199(14)	0	0	0.0036(4)
T	0.75Si + 0.25Al	⅓	⅔	0.1245(5)	0.0180(13)	0.0157(18)	0.0157(18)	0.023(3)	0	0	0.0073(9)
O1	1	⅓	⅔	0	0.021(5)	0.010(6)	0.010(6)	0.043(14)	0	0	0.004(3)
O2	1	0.454(3)	0	0.1700(10)	0.030(3)	0.040(7)	0.021(7)	0.023(7)	0	−0.001(5)	0.010(3)
O3	1	0.629(3)	0	0.4165(8)	0.018(3)	0.022(5)	0.013(6)	0.017(6)	0	0.001(4)	0.006(3)

TABLE 6. Bond distances (Å) for burckhardtite. *A* = (Pb,Ca), *M* = (Te,Fe,Mn) and *T* = (Si,Al).

A−O3:	2.349(12) × 3
A−O2:	3.053(14) × 3
A−O2:	3.442(14) × 3
<*A*−O>:	2.948
M−O3:	1.986(7) × 6
T−O1:	1.621(6) × 1
T−O2:	1.647(5) × 3
<*T*−O>:	1.6405

increase if Pb−O bond valences were larger, so as to correct the slight underbonding of Pb in Table 6. This confirms that these oxygen atoms are O^{2-} rather than OH^-, and along with the absence of O−H bands in Raman spectrum or significant additional electron density peaks, implies that burckhardtite is ideally anhydrous.

Discussion

Crystal structure and chemistry

The crystal structure of burckhardtite is shown in Fig. 2. The true symmetry is trigonal, space group $P\bar{3}1m$. Note that the powder data of Gaines *et al*. (1979) do not demonstrate any deviation from a hexagonal unit-cell metric, in that pairs of reflections such as 11*l* and 02*l* were not resolved. The structure does indeed contain phyllosilicate sheets with 6-rings, but unlike the micas, two such sheets in burckhardtite are linked through apical oxygen atoms with no intervening octahedral sheet, to form an unbranched *zweier* double layer $[AlSi_3O_8]^-$ according to the classification of Liebau (1985). As all oxygen atoms are bridging, substitution of a cation with valence < 4, such as Al^{3+}, is essential to provide a net negative charge on the double sheet. The double sheets are regularly intercalated with dioctahedral sheets, approximately $[(Fe^{3+}Te^{6+})O_6]^{3-}$, which also carry a negative charge. The charge is neutralized by Pb^{2+} ions, which decorate the outside of the dioctahedral sheets and connect them to the aluminosilicate double layers.

The rather regular octahedral coordination of the Te site in the crystal structure indicates that the cation is Te^{6+}, rather than Te^{4+}, as was assumed previously. All Te−O distances are equal (1.986 Å; Table 6) and the standard deviation of O−Te−O bond angles is 6.7°

TABLE 7. Bond valences and bond-valence sums for burckhardtite. Ideal sums for the *A*, *M* and *T* compositions used are 2.00, 4.53 and 3.75 valence units respectively.

	O1	O2	O3	Σ
$A = Pb_{0.97}Ca_{0.03}$		0.1065 ×3→, ×1↓, 0.0480 ×3→, ×1↓	0.4519 ×3→	1.819
$M = Te_{0.51}Fe_{0.38}Mn_{0.11}$			0.7196 ×6→, ×2↓	4.318
$T = Si_{0.75}Al_{0.25}$	1.0272 ×2↓	0.9575 ×3→, ×2↓		3.900
Σ	2.054	2.070	1.891	

(angles are $3 \times 80.3°$, $6 \times 92.8°$ and $3 \times 94.9°$). By contrast, examination of 40 $Te^{4+}O_6$ polyhedra by Christy and Mills (2013) showed them to exhibit much longer mean bond distances covering a broad range (2.241−2.672 Å), as well as larger bond-angle standard deviations (11.6−24.5°). From a bond-valence perspective, if the Te site in burckhardtite were fully occupied by Te, the observed bond distance would yield a bond-valence sum of 5.64 if the Te^{4+}−O bond-valence parameters of Mills and Christy (2013) are used and 5.34 if the Te^{6+}−O parameters are used.

As noted above, the Raman spectrum and structure refinement shows that burckhardtite is anhydrous. Ratios of M^{3+}:Te^{6+} and Al:Si are close to 1:1 and 3:1 respectively, implying that a simplified charge-balanced formula can be written as $Pb_2(Fe^{3+}Te^{6+})[AlSi_3O_8]O_6$. This is consistent with the stoichiometry derived from the crystal structure, although the structure implies that there is no long-range order of (M^{3+},Te) or (Si,Al).

Relationship to other minerals and synthetic compounds

Burckhardtite belongs to a small family of double-sheet phyllosilicate minerals. The simplest examples of these, in which only large cations occur between the silicate double sheets, are the feldspar polymorphs dmisteinbergite, $Ca[Al_2Si_2O_8]$ (Takéuchi and Donnay, 1959; Chesnokov *et al*., 1990) and kokchetavite, $K[AlSi_3O_8]$ (Hwang *et al*., 2004), and their hydrated analogues cymrite, $Ba[Al_2Si_2O_8]\cdot H_2O$ (Drits *et al*., 1975) and 'K-cymrite' (Fasshauer *et al*., 1997; Zhang *et al*., 2009). A more complex example is kampfite, ideally $Ba_{12}[Al_5Si_{11}O_{32}][(CO_3)_{0.875}]_8Cl_5$ (modified slightly from Basciano and Groat, 2007), in which the intersheet region contains a sequence of layers Ba−CO_3–(Ba+Cl)−CO_3−Ba. The tetrahedrally coordinated sites are partially vacant in strätlingite and vertumnite, closely-related minerals with ideal formulae $Ca_2Al[(AlSi\square_2)(O_2(OH)_6\square_2)](OH)_6\cdot 2.25H_2O$ and $Ca_2Al[(AlSi_{1.25}\square_{1.75})(O_3(OH)_5\square_2)](OH)_6\cdot 2.45H_2O$ according to Rinaldi *et al*. (1990). The incomplete double sheets in these minerals are intercalated with a modified brucite-like trioctahedral layer $[Ca_2Al(OH)_6]^{1+}$ of $Al(OH)_6$ octahedra and $Ca(OH)_6(H_2O)$-capped octahedra, very similar to that of the hydrocalumite group of minerals in the hydrotalcite supergroup (Sacerdoti and Passaglia, 1988; Mills *et al*., 2012*b*).

The Si−O−Si angle across the oxygen O1 that bridges the two halves of the double sheet is 180° in burckhardtite. The bond distances and bond-valence sum for O1 imply that this atom is truly located at the special position of point symmetry 32 as in Table 5, rather than dynamically displaced around that position. This is supported by the anisotropy of the displacement parameters, which have $U^{33} > (U^{11}$ and $U^{22})$, implying more displacement along the bond than normal to it. Although such linear coordination is rare for bridging oxygen atoms on the whole, it is a recurrent feature for the central oxygen atoms of double-sheet silicates, occurring also in dmisteinbergite and strätlingite (Takéuchi and Donnay, 1959; Rinaldi *et al*., 1990).

Burckhardtite is the first example of a phase where a complete aluminosilicate double sheet is intercalated with a dioctahedral layer, $[M_2\square X_6]$. If the *M* cations were all Te^{6+} and the *X* anions were all O^{2-}, this sheet would be electrostatically neutral, but as in the aluminosilicate part of the structure, a net negative charge is provided by substitution of lower-valent cations, primarily Fe^{3+} in this case. Each *X* anion is bonded to only two *M* cations, which allows the possibility

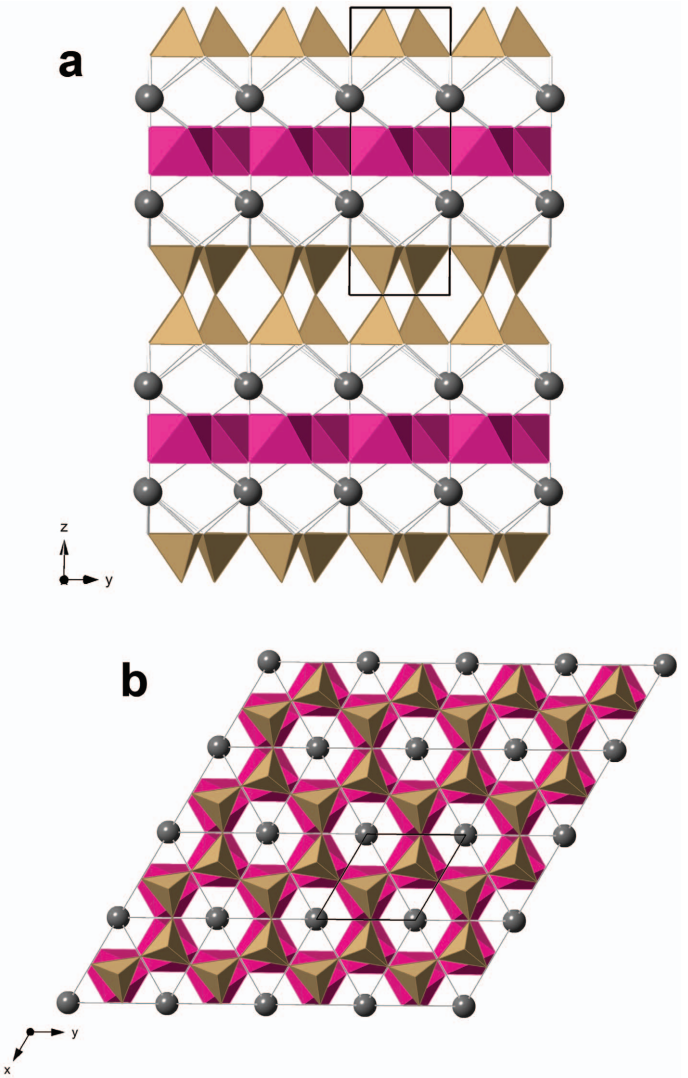

FIG. 2. Crystal structure of burckhardtite viewed (*a*) down **x** and (*b*) down **z**. (Fe,Te) octahedra are red, (Si,Al) tetrahedra are brown and Pb atoms are grey spheres. Unit cell outlined in black.

of maintenance of a constant bond-valence sum on the anions by strict alternation of the two types of *M* cation. The large difference in valence between Te and Fe implies that such ordering would be favourable, and the observed Te:M^{3+} ratio ≈ 1:1 strongly suggests that the octahedrally coordinated cations do order within a given layer. However, there is no evidence of ordering in the third dimension, presumably because of the wide separation between successive octahedral layers. This situation is analogous to that in the layered double hydroxide phases of the hydrotalcite supergroup, where two octahedrally coordinated cations may order strongly within a brucite-like layer, but decoupling between layers means that evidence of three-dimensional long-range order is rarely, if at all, observed (e.g. Mills *et al*., 2012*b*, Génin *et al*., 2014). In the single-crystal diffraction pattern of burckhardtite, we observed no streaks or diffuse scattering that might indicate additional short-range order.

The tetrahedral double layer $[AlSi_3O_8]^-$ and trioctahedral sheet $[Fe^{3+}Te^{6+}O_6]^{3-}$ of burckhardtite are both anionic. The charge is balanced

by layers of Pb^{2+} cations which lie between a tetrahedral double sheet on one side and a dioctahedral layer on the other. Pb is in 3+3+3 coordination, forming three short bonds to O3 in the octahedral layer and six longer bonds to O2 in the tetrahedral double sheet (Table 6, Fig. 3). The Pb^{2+} lone pair is evidently directed along ±**z** towards the centre of the ditrigonal silicate rings.

The Pb−[M_2X_6]−Pb compound layer of burckhardtite can be regarded as a slab of rosiaite-like structure intercalated with the tetrahedral double sheet. Rosiaite ($PbSb_2O_6$) has the same $P\bar{3}1m$ space group as burckhardtite and a very similar *a* parameter (5.295 Å). It has a structure in which two types of octahedrally coordinated cations occupy alternately ⅓ or ⅔ of the available sites between alternate layers of a hexagonal close-packed anion array (Basso *et al*., 1996), corresponding to the Li_2ZrF_6 (= $ZrLi_2F_6$) archetype (Brunton, 1973), albeit with different relative valences of the two types of cation. We note that synthetic $PbSb_2O_6$ was reported initially to have a slight distortion of this structure type (*P*312 space group; Magnéli, 1941). In rosiaite, where the Pb-site symmetry is centrosymmetric $\bar{3}m$ and the Pb atom is sandwiched between two M_2X_6 layers, the Pb coordination polyhedron is nearly regular octahedral with six equivalent Pb−O distances of 2.554 Å and lone-pair stereoactivity is suppressed. However, in burckhardtite, there is a M_2X_6 layer on only one side of the Pb site which, hence, has polar 3*m* point symmetry; much longer bonds are made to the O atoms of the aluminosilicate sheet on the other side (Table 6, Fig. 3), consistent with the lone pair orienting in this direction, as noted above.

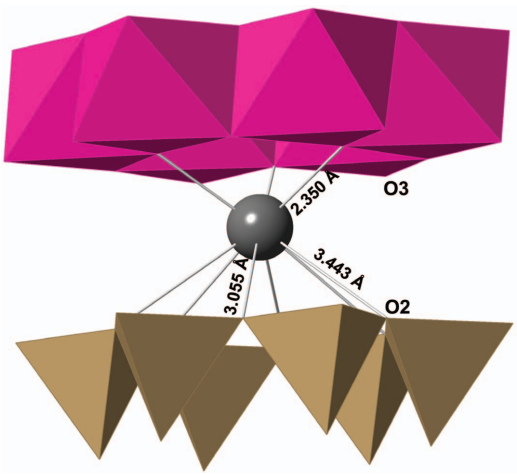

FIG. 3. The Pb environment in burckhardtite, showing Pb (grey sphere), three short bonds to O3 and 3 + 3 longer bonds to O2. The lone pair of the Pb atom is directed towards the centre of the aluminosilicate 6-ring (brown).

Phyllotellurate M_2O_6 layers very similar to that of burckhardtite, with 1:1 substitution of Te^{6+} and a lower-valence *M* cation ensuring a net negative charge overall, are known from several synthetic tellurates with the $PbSb_2O_6/Li_2ZrF_6$ topology. However, in all of these cases, the two types of high-valence cations are long-range ordered to produce superstructures. They include $SrGeTeO_6$, where ordering lowers the symmetry to *P*312, and a suite of compounds *REE*$CrTeO_6$ (*REE* = La−Yb and Y; Kasper, 1969) plus $LaFeTeO_6$ (Phatak *et al*., 2010) with a doubled *c* repeat and $P\bar{3}1c$ symmetry (isostructural with colquiriite, $CaLiAlF_6$; Yin and Keszler, 1992). $LaFeTeO_6$, in particular, has a $[Fe^{3+}Te^{6+}O_6]^{3-}$ layer that is identical compositionally to the substituted phyllotellurate layer of burckhardtite. Similar layers with varying degrees of cation disorder also occur in the compounds $Na_{2-x}[(Te,Sn)_2O_6]$, $Na_2[GeTeO_6]$ and $Na_2[TiTeO_6]$ with the ilmenite structure (Woodward *et al*., 1999), while a fully disordered phyllotellurate layer with cations in trigonal prismatic coordination rather than octahedral coordination was reported for $Sr[MnTeO_6]$ by Wulff and Müller-Buschbaum (1998).

Acknowledgements

The authors thank Fernando Cámara, Peter Leverett, Peter Williams and an anonymous reviewer for helpful suggestions which improved the manuscript. Part of this study has been funded by the Ian Potter Foundation grant "tracking tellurium" to SJM which we acknowledge gratefully. The X-ray diffraction study was funded by the John Jago Trelawney Endowment to the Mineral Sciences Department of the Natural History Museum of Los Angeles County and microprobe and Raman analyses were funded by a grant from the Northern California Mineralogical Association.

References

Basciano, L.C. and Groat, L.A. (2007) The crystal structure of kampfite. *The Canadian Mineralogist*, **45**, 935−943.

Basso, R., Lucchetti, G., Zefiro, L. and Palenzona, A. (1996) Rosiaite, $PbSb_2O_6$, a new mineral from the

Cetine mine, Siena, Italy. *European Journal of Mineralogy*, **8**, 487–492.

Brese, N.E. and O'Keeffe, M. (1991) Bond-valence parameters for solids. *Acta Crystallographica*, **B47**, 192–197.

Brunton, G. (1973) Li_2ZrF_6. *Acta Crystallographica*, **B29**, 2294–2296.

Burla, M.C., Caliandro, R., Camalli, M., Carrozzini, B., Cascarano, G.L., De Caro, L., Giacovazzo, C., Polidori, G. and Spagna, R. (2005) *SIR2004*: an improved tool for crystal structure determination and refinement. *Journal of Applied Crystallography*, **38**, 381–388.

Chesnokov, B.V., Lotova, E.V., Nigmatulina, E.N., Pavlyuchenko, V.S. and Bushmakin, A.F. (1990) Dmisteinbergite $CaAl_2Si_2O_8$ (hexagonal) – a new mineral. *Zapiski Vsesoyuznogo Mineralogicheskogo Obshchestva*, **119**, 43–46 [in Russian].

Christy, A.G. and Mills, S.J. (2013) Effect of lone-pair stereoactivity on polyhedral volume and structural flexibility: application to $Te^{IV}O_6$ octahedra. *Acta Crystallographica*, **B69**, 446–456.

Drits, V.A., Kashaev, A.A. and Sokolova, G.V. (1975) Crystal-structure of cymrite. *Kristallografiya*, **20**, 280–286 [in Russian].

Fasshauer, D.W., Chatterjee, N.D. and Marler, B. (1997) Synthesis, structure, thermodynamic properties, and stability relations of K-cymrite, $K[AlSi_3O_8]\cdot H_2O$. *Physics and Chemistry of Minerals*, **24**, 455–462.

Fintor, K., Walter, H. and Nagy, Sz. (2013) Petrographic and micro-Raman analysis of chondrules and (Ca,Al)-rich inclusions of NWA 2086 CV3 type carbonaceous chondrite. *Lunar and Planetary Science*, **44**, 1152.

Gaines, R.V., Leavens, P.B. and Nelen, J.A. (1979) Burckhardtite, a new silicate-tellurite from Mexico. *American Mineralogist*, **64**, 355–358.

Génin, J.-M.R., Mills, S.J., Christy, A.G., Guérin, O., Herbillon, A.J., Kuzmann, E., Ona-Nguema, G., Ruby, C. and Upadhyay, C. (2014) Mössbauerite, $Fe_6^{3+}O_4(OH)_8[CO_3]\cdot 3H_2O$, the fully oxidized 'green rust' mineral from Mont Saint-Michel Bay, France. *Mineralogical Magazine*, **78**, 447–465.

Graham, C.M., Tareen, J.A.K., McMillan, P.F. and Lowe, B.M. (1992) An experimental and thermodynamic study of cymrite and celsian stability in the system $BaO–Al_2O_3–SiO_2–H_2O$. *European Journal of Mineralogy*, **4**, 251–269.

Higashi, T. (2001) *ABSCOR*. Rigaku Corporation, Tokyo.

Hwang, S.-L., Shen, P., Chu, H.-T., Yui, T.-F., Liou, J.G., Sobolev, N.V., Zhang, R.-Y., Shatsky, V.S. and Zayachkovsky, A.A. (2004) Kokchetavite: a new potassium-feldspar polymorph from the Kokchetav ultrahigh-pressure terrane. *Contributions to Mineralogy and Petrology*, **148**, 380–389.

Ibers, J.A. and Hamilton, W.C. (editors) (1974) *International Tables for X-ray Crystallography*, Vol. IV. Kynock, Dordrecht, The Netherlands, 366 pp.

Kampf, A.R., Housley, R.M., Mills, S.J., Marty, J. and Thorne, B. (2010) Lead-tellurium oxysalts from Otto Mountain near Baker, California: I. Ottoite, Pb_2TeO_5, a new mineral with chains of tellurate octahedra. *American Mineralogist*, **95**, 1329–1336.

Kampf, A.R., Mills, S.J., Housley, R.M., Rossman, G.R., Marty, J. and Thorne, B. (2013*a*) Lead-tellurium oxysalts from Otto Mountain near Baker, California: X. Bairdite, $Pb_2Cu_4^{2+}Te_2^{6+}O_{10}(OH)_2(SO_4)(H_2O)$, a new mineral with thick HCP layers. *American Mineralogist*, **98**, 1315–1321.

Kampf, A.R., Mills, S.J., Housley, R.M., Rossman, G.R., Marty, J. and Thorne, B. (2013*b*) Lead-tellurium oxysalts from Otto Mountain near Baker, California: XI. Eckhardite, $(Ca,Pb)Cu^{2+}Te^{6+}O_5(H_2O)$, a new mineral with HCP stair-step layers. *American Mineralogist*, **98**, 1617–1623.

Kanzaki, M., Xue, X., Amalberti, J. and Zhang, Q. (2012) Raman and NMR spectroscopic investigation of high-pressure K-cymrite ($KAlSi_3O_8\cdot H_2O$) and its anhydrous form (kokchetavite). *Journal of Mineralogical and Petrological Sciences*, **107**, 114–119.

Kasper, H.M. (1969) $LnCrTeO_6$ – a new series of compounds based on the $PbSb_2O_6$ structure. *Materials Research Bulletin*, **4**, 33–37.

Krivovichev, S.V. and Brown, I.D. (2001) Are the compressive effects of encapsulation an artifact of the bond valence parameters? *Zeitshcrift für Kristallographie*, **216**, 245–247.

Liebau, F. (1985) *Structural Chemistry of Silicates: Structure, Bonding and Classification*. Springer-Verlag, New York, 347 pp.

Magnéli, A. (1941) The crystal structure of lead metaantimonate and isomorphous compounds. *Arkiv för Kemi, Mineralogi och Geologi*, **B15**, 1–6.

Mills, S.J., Bindi, L., Cadoni, M., Kampf, A.R., Ciriotti, M.E. and Ferraris, G. (2012*a*) Paseroite, $PbMn^{2+}(Mn^{2+},Fe^{2+})_2(V^{5+},Ti,Fe^{3+},\square)_{18}O_{38}$, a new member of the crichtonite group. *European Journal of Mineralogy*, **24**, 1061–1067.

Mills, S.J., Christy, A.G., Kameda, T., Génin, J.-M.R. and Colombo, F. (2012*b*) Nomenclature of the hydrotalcite supergroup: natural layered double hydroxides. *Mineralogical Magazine*, **76**, 1289–1336.

Mills, S.J. and Christy, A.G. (2013) Revised values of the bond valence parameters for $Te^{IV}–O$, $Te^{VI}–O$ and $Te^{IV}–Cl$. *Acta Crystallographica*, **B69**, 145–149.

Mills, S.J., Kampf, A.R., Christy, A.G., Housley, R.M., Rossman, G.R., Reynolds, R.E. and Marty, J. (2014)

Bluebellite and mojaveite, two new minerals from the central Mojave Desert, California, USA. *Mineralogical Magazine*, **78**, 1325–1340.

Phatak, R., Krishnan, K., Kulkarni, N.K., Achary, S.N., Banerjee, A. and Sali, S.K. (2010) Crystal structure, magnetic and thermal properties of $LaFeTeO_6$. *Materials Research Bulletin*, **45**, 1978–1983.

Rinaldi, R., Sacerdoti, M. and Passaglia, E. (1990) Strätlingite: crystal structure, chemistry, and a reexamination of its polytype vertumnite. *European Journal of Mineralogy*, **2**, 841–849.

Sacerdoti, M. and Passaglia, E. (1988) Hydrocalumite from Latium, Italy – its crystal structure and relationship with related synthetic phases. *Neues Jahrbuch für Mineralogie Monatshefte*, **1988**, 462–475.

Sheldrick, G.M. (2008) A short history of *SHELX*. *Acta Crystallographica*, **A64**, 112–122.

Takéuchi, Y. and Donnay, G. (1959) The crystal structure of hexagonal $CaAl_2Si_2O_8$. *Acta Crystallographica*, **12**, 465–470.

Walstrom, R.E. (2012) "The Accidental Pocket, Cochise County, Arizona". Northern California Mineralogical Society Annual Meeting, 2012. Cited in http://www.mindat.org/min-804.html. Accessed on 18 June 2014.

Woodward, P.M., Sleight, A.W., Du, L.-S. and Grey, C.P. (1999) Structural studies and order-disorder phenomenon in a series of new quaternary tellurates of the type $A^{2+}M^{4+}Te^{6+}O_6$ and $A_2^{1+}M^{4+}Te^{6+}O_6$. *Journal of Solid State Chemistry*, **147**, 99–116.

Wulff, L. and Müller-Buschbaum, H. (1998) Isolierte trigonale SrO_6–Prismen verknüpfen Kagomé-Netze im Strontium-Manganat(IV)-Tellurat(VI): $SrMnTeO_6$. *Zeitschrift für Naturforschung, B: A Journal in Chemical Sciences*, **53**, 283–286.

Yin, Y.B. and Keszler, D.A. (1992) Crystal-chemistry of colquiriite-type fluorides. *Chemistry of Materials*, **4**, 645–648.

Zhang, R.Y., Liou, J.G., Iizuka, Y. and Yang, J.S. (2009) First record of K-cymrite in North Qaidam UHP eclogite, Western China. *American Mineralogist*, **94**, 222–228.